International Journal of Infectious Diseases 82 (2019) 138–146

Contents lists available at ScienceDirect

International Journal of Infectious Diseases

journal homepage: www.elsevier.com/locate/ijid

MRI evaluation of pulmonary lesions and lung tissue changes induced by tuberculosis

Jianbing Zeng[a,1], Zhou Liu[b,c,d,1], Guanle Shen[e], Yuzhong Zhang[a], Li Li[d], Zhiqing Wu[a], Dehong Luo[d], Qingping Gu[f], Hui Mao[c,**], Liya Wang[a,b,c,*]

[a] Department of Radiology, The People's Hospital of Longhua, Shenzhen, Southern Medical University, Guangdong, China
[b] Graduate School, Medical College of Nanchang University, Nanchang, Jiangxi, China
[c] Department of Radiology and Imaging Sciences, Emory University School of Medicine, Atlanta, Georgia, USA
[d] Department of Radiology, National Cancer Center/National Clinical Research Center for Cancer/Cancer Hospital & Shenzhen Hospital, Chinese Academy of Medical Sciences and Peking Union Medical College, Shenzhen, China
[e] Department of Respiratory, People's Hospital of Longhua, Shenzhen, Guangdong, China
[f] Department of Marketing, Philips Medical Systems Greater China, China

ARTICLE INFO

Article history:
Received 30 November 2018
Received in revised form 4 March 2019
Accepted 4 March 2019
Corresponding Editor: Eskild Petersen, Aarhus, Denmark

Keywords:
Magnetic resonance imaging
Lung
Computed tomography
Pulmonary tuberculosis
Motion correction

ABSTRACT

Objective: To evaluate the utility of magnetic resonance imaging (MRI) with an advanced motion correction technique in characterizing lung tissue changes and lesions induced by pulmonary tuberculosis (TB).

Methods: Sixty-three subjects with computed tomography (CT) features of pulmonary TB underwent lung MRI. All subjects with pulmonary TB were confirmed by acid-fast bacillus (AFB) testing or the detection of *Mycobacterium tuberculosis*. T2-weighted turbo spin echo (TSE) sequence MRI with the MultiVane motion correction technique was used to image the lungs. Routine lung CT images were obtained as reference. MRI and CT images were reviewed by multiple readers independently. The performance of MRI in depicting abnormalities induced by pulmonary TB and their morphological changes were evaluated and compared with the performance of CT.

Results: Lung MRI found pulmonary abnormalities in all 63 TB subjects, with satisfactory quality. With the implementation of MultiVane for T2-weighted TSE sequences to reduce the motion correction effect, MRI showed excellent agreement with CT in detecting abnormal imaging features of pulmonary TB ($\kappa = 0.88$, $p < 0.001$), such as tree-in-bud sign, ground-glass opacity, consolidation, mass, and cavitation. MRI was advantageous in identifying caseation and liquefactive necrosis based on inhomogeneous signal distribution within consolidations and also in identifying mild pleural effusion. The optimized lung MRI was comparable to CT in detecting non-calcified nodules ($\kappa = 0.90$), with overall sensitivity of 50.0%, 91.1%, and 100% for nodules of size <5 mm, 5–10 mm, and >10 mm, respectively. However, MRI was less effective in identifying lesions with calcification.

Conclusions: The clinical implementation of an optimized MRI protocol with the MultiVane motion correction technique for imaging pulmonary TB is feasible. Lung MRI without ionizing radiation is a promising alternative to the clinical standard CT, especially for pregnant women, children, adolescents, and patients requiring short-term and repeated follow-up observations.

Introduction

According to the Global Tuberculosis Report of 2017, tuberculosis (TB) is the leading cause of death from infectious disease, above HIV/AIDS, and the ninth leading cause of death among all diseases (World Health Organization, 2016). This is despite the fact that early diagnosis and effective treatment have long been available. In 2016, there were an estimated 10.4 million new TB cases, with children (age <15 years) accounting for 6.9% (World

* Corresponding author at: Department of Radiology, The People's Hospital of Longhua, Shenzhen, Southern Medical University, 38 Jinglong Jianshe Road, Longhua, Shenzhen, Guangdong 518109, China.
** Corresponding author at: Department of Radiology and Imaging Sciences, Emory University School of Medicine, 1841 Clifton Road, Atlanta, Georgia 30329, USA.
E-mail addresses: hmao@emory.edu (H. Mao), lwang30@emory.edu (L. Wang).
[1] Jianbing Zeng and Zhou Liu contributed equally to this work.

https://doi.org/10.1016/j.ijid.2019.03.004

Health Organization, 2016). Most deaths from TB could be averted with early diagnosis and appropriate treatment.

With low cost and a relatively low radiation dose, plain chest X-ray radiography has historically been the most common imaging test used to evaluate pulmonary TB. X-ray computed tomography (CT), regarded as the standard method for characterizing lung lesions, has increasingly been used for the diagnosis of TB and its complications (Muller, 2002), offering three-dimensional and high resolution imaging for the detection and quantification of lesions. However, alternative imaging methods without ionizing radiation have been sought in recent years, largely due to concerns about the effect of ionizing radiation for vulnerable populations such as children, pregnant women, and patients requiring repeated and frequent follow-up (Liszewski et al., 2017; Rizzi et al., 2011).

Magnetic resonance imaging (MRI) is a commonly used non-ionizing three-dimensional diagnostic imaging modality with superb resolution and exquisite soft tissue contrast in lesion detection and functional measurements. It is widely available in most hospitals. However, lung MRI is not well accepted clinically due to the concern of poor image quality caused by low proton density in the lung, rapid signal decay due to high magnetic susceptibility at the air–tissue interface, and intrinsic motion artifacts from respiratory and cardiac motions (Cutillo et al., 1995). Tissue loss as a result of the disease, hyperinflation, and hypoxic hypo-perfusion, e.g., in emphysema or so-called 'minus-pathology', are also common problems in lung MRI (Iwasawa et al., 2007; Wielputz and Kauczor, 2012). With developments in parallel imaging and under-sampling methods that accelerate image acquisition and reduce air-caused susceptibility artifacts to preserve signals, MRI protocols can be optimized with tailored sequences and parameters to gain sufficient image quality to evaluate abnormalities in the lung (Biederer et al., 2012). T2-weighted turbo spin echo (TSE) imaging has been used in previous studies to demonstrate lung imaging and lesion detection (Biederer et al., 2012; Eibel et al., 2006; Leutner et al., 2000; Wild et al., 2012).

With the improved motion correction techniques available for clinical use, such as MultiVane, there has been increasing interest and effort in applying MRI for the study of lung diseases. MRI images are typically formed by filling k-space with spatially encoded data points line-by-line, in the order of a Cartesian method in Cartesian coordinates. The MultiVane technique is capable of correcting in-plane rotation and translation due to patient movement by recording data in a hybrid k-space trajectory, which is a combination of Cartesian and radial directions. The sets of Cartesian acquired lines of data points in k-space are like 'vanes'. MultiVane is particularly designed because an individual vane is a Cartesian dataset. Each vane contains k-space samples corresponding to the same low resolution image. All vanes are ultimately combined to create a single high-resolution image that is sharp and artifact-free. If the low resolution image from a specific vane correlates poorly with other vanes, for example due to motion, it is eliminated or underweighted during reconstruction. The MultiVane technique with non-Cartesian k-space sampling combined with parallel imaging has been shown to significantly reduce motion artifacts caused by cardiac and respiratory motion (Meier-Schroers et al., 2016). Thus, the quality of lung imaging and the sensitivity of lesion detection are increased even without the patient holding their breath. Although this technique has been demonstrated in the evaluation of several lung diseases (Attenberger et al., 2014; Chung et al., 2013, 2016; Dewes et al., 2016; Ekinci et al., 2017; Liszewski et al., 2017; Nagel et al., 2016; Ozcan et al., 2017; Puderbach et al., 2007), its application in the evaluation of pulmonary TB by MRI has not been explored.

This study was performed to investigate the utility of the MultiVane technique implemented in the lung MRI protocol in the diagnosis of pulmonary TB and its diagnostic performance, by comparing the results with those of CT examinations performed on the same subjects. The results demonstrated that various TB-induced pulmonary abnormalities can be readily detected and quantified by MRI, with image quality and interpretability comparable to those of CT. Furthermore, MRI offers several advantages over CT in the detection and characterization of consolidation with caseous necrosis or liquefactive necrosis, but has limitations in depicting calcified lesions. The study demonstrated that MRI can be an alternative method to the clinical standard CT, with potential advantages for imaging patients who are vulnerable to CT radiation such as pregnant women, children, adolescents, and patients requiring repeated follow-up observations.

Subjects and methods

Subjects and clinical information

This prospective study was performed from December 2017 to August 2018 and was approved by the institutional review board (IRB). All participants, including healthy subjects and patients, provided informed consent to participate in this study. Ten healthy participants underwent lung MRI to test and confirm the optimized MRI protocol, through the comparison of T2-weighted TSE sequences with/without the MultiVane technique. Sixty-three patients with pulmonary TB, including 50 male patients (79.4%) and 13 female patients (20.6%) with a mean age of 39 ± 15 years (range 17–75 years), were enrolled in this study. They were all diagnosed based on positive thoracic CT findings followed by confirmation by acid-fast bacillus (AFB) testing or the detection of *Mycobacterium tuberculosis* in sputum. All patients were recruited after their routine examination at the clinical visit. They were not receiving any treatment at the time of MRI, and had not received any treatment during 1 year prior to the time of MRI. Based on clinical evaluation and imaging features, 42 patients had active TB and 21 patients had inactive TB. All patients had received or were receiving anti-TB treatment after diagnosis. Enrolled subjects were screened for MRI safety before undergoing MRI, which was performed within 48 hours following the CT examination. Detailed information on the study subjects is summarized in Table 1.

Table 1
Demographic information for the study patients.

Item	Subjects in different categories
Male	50
Female	13
Age (years), mean ± SD	39 ± 15 (range 17–75)
TB type	
Active pulmonary TB	42
Old inactive pulmonary TB	21
Treatment status	
Initial untreated	30
Recurrence after treatment withdrawal (more than 1 year)	12
Old inactive after treatment withdrawal (more than 1 year)	21
Lesion location (lung lobe)	
Right upper lobe (cases)	47
Right middle lobe (cases)	10
Right lower lobe (cases)	14
Left upper lobe (cases)	39
Left lower lobe (cases)	16
Total affected lobes	126/315
MRI artifact score	
1 (cases)	31
2 (cases)	24
3 (cases)	8
4 (cases)	0
Total MRI scans	63

SD, standard deviation; TB, tuberculosis; MRI, magnetic resonance imaging.

Lung MRI protocol

All lung MRI images were obtained using a 1.5T whole-body MRI scanner (Achieva, Philips Healthcare, Best, the Netherlands) with a 4-element body wrap coil. First, a direct comparison was made between the T2-weighted TSE images with MultiVane technique implemented and the routine T2-weighted TSE images without MultiVane technique implemented obtained from the 10 healthy subjects. All 63 TB subjects then underwent MRI, and T2-weighted TSE sequences with MultiVane implemented were obtained for comparison with CT.

The T2-weighted TSE sequence protocol with MultiVane and respiratory triggering was performed in coronal and axial sections using an echo time (TE) of 85/100 ms, TSE factor = 33, flip angle = 180/90°, and phase resolution = 80%, with slice thickness of 5 mm, field of view (FOV) = 400 × 400 mm, matrix size = 308 × 308, and with free breathing. For the respiratory triggered scan, the actual repetition time (TR) was determined based on the respiratory rhythm of each subject, which was typically in the range of 2000–4000 ms. The FOV coverage was from the pulmonary apex to the costophrenic angle. The whole acquisition time for the lung MRI examination was typically 12 minutes. In order to simplify the protocol and shorten the acquisition time, a T1-weighted spin echo sequence was not included in the lung MRI protocol applied to this cohort.

The signal-to-noise ratio (SNR) and contrast-to-noise ratio (CNR) in selected regions of interest (ROIs) were calculated for comparison of lung MRI imaging quality between T2-weighted imaging with MultiVane and routine T2-weighted imaging with and without fat suppression. Signal intensities (SI) of ROIs selected in normal pulmonary parenchyma (SI_{normal}) and those from the latissimus dorsi muscle (SI_{muscle}) were measured to compare with background standard deviation (SD) in the same slice. SNR was then computed using the formulas: $SNR = SI_{normal}/SD$ and $CNR = SI_{muscle} - SI_{normal}/SD$.

The quality of MRI images was rated based on a four-point scoring scale reported previously (Eibel et al., 2006; Leutner et al., 2000), i.e., score 1: no artifacts in images; score 2: a few negligible artifacts that do not affect its diagnostic value; score 3: image with diagnostic value but impaired by artifacts; score 4: image with limited diagnostic value due to severe artifacts.

CT protocol

All CT images were obtained using a 256-row multi-detector CT scanner (Revolution CT, GE Medical systems, Milwaukee, WI, USA) without any contrast medium. The following imaging parameters were applied: slice thickness = 5 mm, collimation = 64 × 0.6 mm, voltage = 120 kVp, tube current setting = 20 mAs, matrix size = 512 × 512, reconstruction interval = 1.25 mm at a helical pitch of 1. For comparison with MRI images, the CT images were reformatted to a slice thickness of 5 mm, with imaging volume from the pulmonary apex to the costophrenic angle, similar to the MRI coverage. CT imaging was performed with the patient holding their breath. The total acquisition time was 10 seconds, without the preparation time. The lung window (level: −600, width: 1500) was set to assess the lung parenchyma, while the mediastinal window (level: 30, width: 350) was used to show calcification and pleural effusion.

Comparison of image quality of MRI with CT

To evaluate and validate lung MRI findings, both CT and MRI images were read and compared on workstations running a picture archiving and communication system (PACS) by four radiologists with 2–5 years of lung imaging experience. In order to eliminate the bias from any prior knowledge of the cases during this evaluation, two of the readers were assigned to only read and evaluate CT images and the other two were only responsible for reading and evaluating the MRI images. They performed their evaluations independently and were blinded to the reports of the others. When combining the results, any discrepancy was investigated through consultation with two senior radiologists with more than 25 years of experience in lung imaging interpretation. A total of six radiologists were involved in the evaluation of pulmonary lesions in this study. Disagreements were discussed until a consensus was reached.

For each section of the lung lobes, including two on the left and three on the right, the presence of pulmonary abnormalities, their location and size, and characteristics of the lesions were viewed in both CT and MRI images and documented individually. MRI features of pulmonary TB abnormalities were identified and interpreted with respect to the tree-in-bud sign, centrilobular nodules, ground-glass opacity, finger-in-glove sign, consolidation, interstitial infiltrates, nodules and mass, cavity, liquefactive necrosis, caseous necrosis, pleural involvement effusion, and enlarged lymph nodes, as used conventionally for the interpretation of CT findings. Regarding the criterion of 'nodule and mass', a round lesion with a diameter of 3 cm or smaller in the pulmonary parenchyma was defined as a nodule, while a lesion with a diameter larger than 3 cm was defined as a mass, both for CT and MRI (Rizzi et al., 2011). The size of a nodule was measured as the largest diameter and/or the largest area measured from the selected image slice on CT using the toolbox provided in the PACS workstation. Nodules were classified into non-calcified nodules, partially calcified nodules, or completely calcified nodules.

Statistical analysis

The statistical analysis was performed using IBM SPSS Statistics version 19.0 (IBM Corp., Armonk, NY, USA). A two-tailed paired *t*-test was used to compare the difference in SI between the optimized and routine T2-weighted MRI. Cohen's kappa coefficient (κ) was calculated to assess the degree of agreement between the image findings from CT and MRI images. A κ value of <0.00 was considered to indicate poor agreement. A κ value of 0.00–0.20, 0.21–0.40, 0.41–0.60, and 0.61–0.80 was considered to indicate slight, fair, moderate, and substantial agreement, respectively. A value within 0.81–1.00 was considered to indicate excellent agreement (Landis and Koch, 1977).

The sensitivity of MRI for the detection of different types of nodules was calculated as the ratio of detection with 95% confidence interval (CI). Differences in sensitivity of nodule detection were evaluated by Chi-square test (Pearson's Chi-square test and Fisher's exact test). A value of $p < 0.05$ was considered statistically significant.

Results

Improvement in lung MRI quality

T2-weighted TSE imaging with MultiVane implemented demonstrated that the MultiVane technique significantly improved the lung MRI image quality, with reduced respiratory and cardiac motion artifacts (Figure 1A–D). As summarized in Table 1, for the total 63 patients with pulmonary TB, there were 31 cases (49.2%) with no artifact (score 1), 24 cases (38.1%) with minimal artifacts that did not affect its diagnostic value (score 2), and eight cases (12.7%) with images of diagnostic value but impaired by artifacts (score 3); none of the cases had a score of 4 indicating limited diagnostic value due to severe artifacts. Table 2 presents the SNR and CNR of pulmonary parenchyma, which were increased for T2-weighted TSE imaging with MultiVane implemented

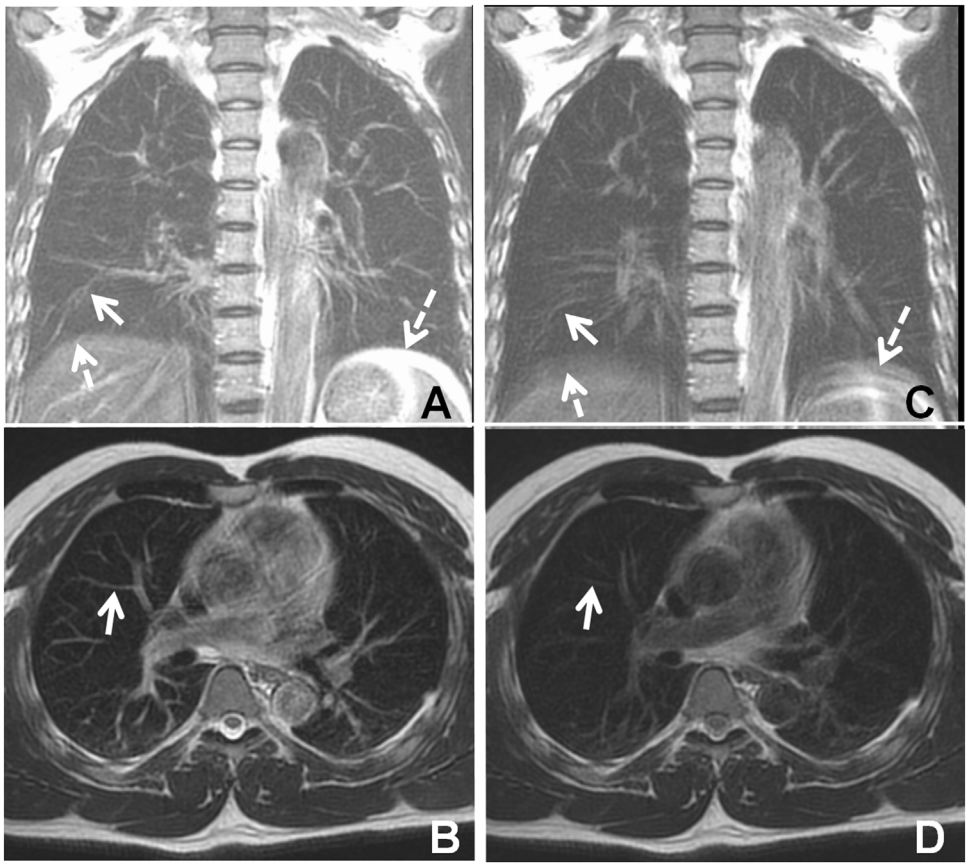

Figure 1. Comparison of MultiVane and routine T2-weighted TSE images. T2-weighted TSE imaging with the MultiVane technique clearly depicts the pulmonary vasculature and bronchi (arrows) in both coronal (A) and axial (B) sections, when compared with both structures recorded without the MultiVane technique, as shown in images (C) and (D). Additionally, the surface of the diaphragm can be seen as a smooth margin in image (A), but is unclear with multiple shadows (dashed arrow) in image (C). The image contrast window was adjusted purposely to that of conventional CT images for the evaluation of lung structures and lesions.

Table 2
Comparison of T2 TSE image quality with and without MultiVane.[a]

Image quality measurement	With MultiVane	Without MultiVane	*p*-Value
SNR			
Right	62.07 ± 13.59	36.56 ± 6.66	<0.0001
Left	62.27 ± 6.10	36.43 ± 9.54	<0.0001
CNR			
Right	604.35 ± 136.02	351.78 ± 66.59	<0.0001
Left	606.33 ± 61.36	350.43 ± 95.23	<0.0001

T2 TSE, T2-weighted turbo spin echo sequence; SNR, signal-to-noise ratio; CNR, contrast-to-noise ratio; ROIs, regions of interest.
[a] Image quality was evaluated based on SNR and CNR measured from the ROIs selected from the right or left pulmonary parenchyma.

compared to routine T2-weighted TSE imaging without MultiVane ($p < 0.0001$).

Comparison between MRI and CT in detecting lung abnormalities

Given MRI and CT have their respective strengths and weaknesses in identifying imaging features of lung abnormalities, a direct comparison of the lesion characterization and diagnostic performance was made between MRI and CT in the same subjects. Table 3 summarizes the pulmonary TB abnormalities found by MRI and CT in the 63 patients with pulmonary TB, as well as the levels of agreement. In general, diagnostic information and reports from images obtained by MRI with MultiVane implemented showed strong agreement with those from CT in the detection of several common lung abnormalities (Figure 2). Typical pulmonary TB presents multiple lesions with different (or distinct) radiological or imaging features, such as tree-in-bud sign (κ = 1), ground-glass opacity sign (κ = 0.90), finger-in-glove sign (κ = 1), interstitial change (κ = 1), consolidation (κ = 1), cavitation (κ = 1), and mass (κ = 1) in the current study.

It should be noted that MRI demonstrated significant advantages in providing additional imaging features inside consolidations, such as caseous necrosis and liquefactive necrosis. However,

Table 3
Comparison of MRI and CT in the detection of various abnormalities induced by pulmonary TB.

Abnormalities	MRI (cases)	CT (cases)	κ value	Advantage
Consolidation	22	22	1	–
Mass	10	10	1	–
Alteration consistent with caseous necrosis	4	0	0	MRI
Alteration consistent with liquefactive necrosis	7	0	0	MRI
Cavitation	16	16	1	–
Ground-glass opacity	5	6	0.87	CT
Nodule	38	41	0.88	CT
Tree-in-bud sign	30	30	1	–
Interstitial change	21	21	1	–
Pleural involvement	46	43	0.87	MRI
Pleural effusion	16	7	0.52	MRI
Bronchiectasis	2	3	0.79	CT
Finger-in-glove sign	1	1	1	–

MRI, magnetic resonance imaging; CT, computed tomography; TB, tuberculosis.

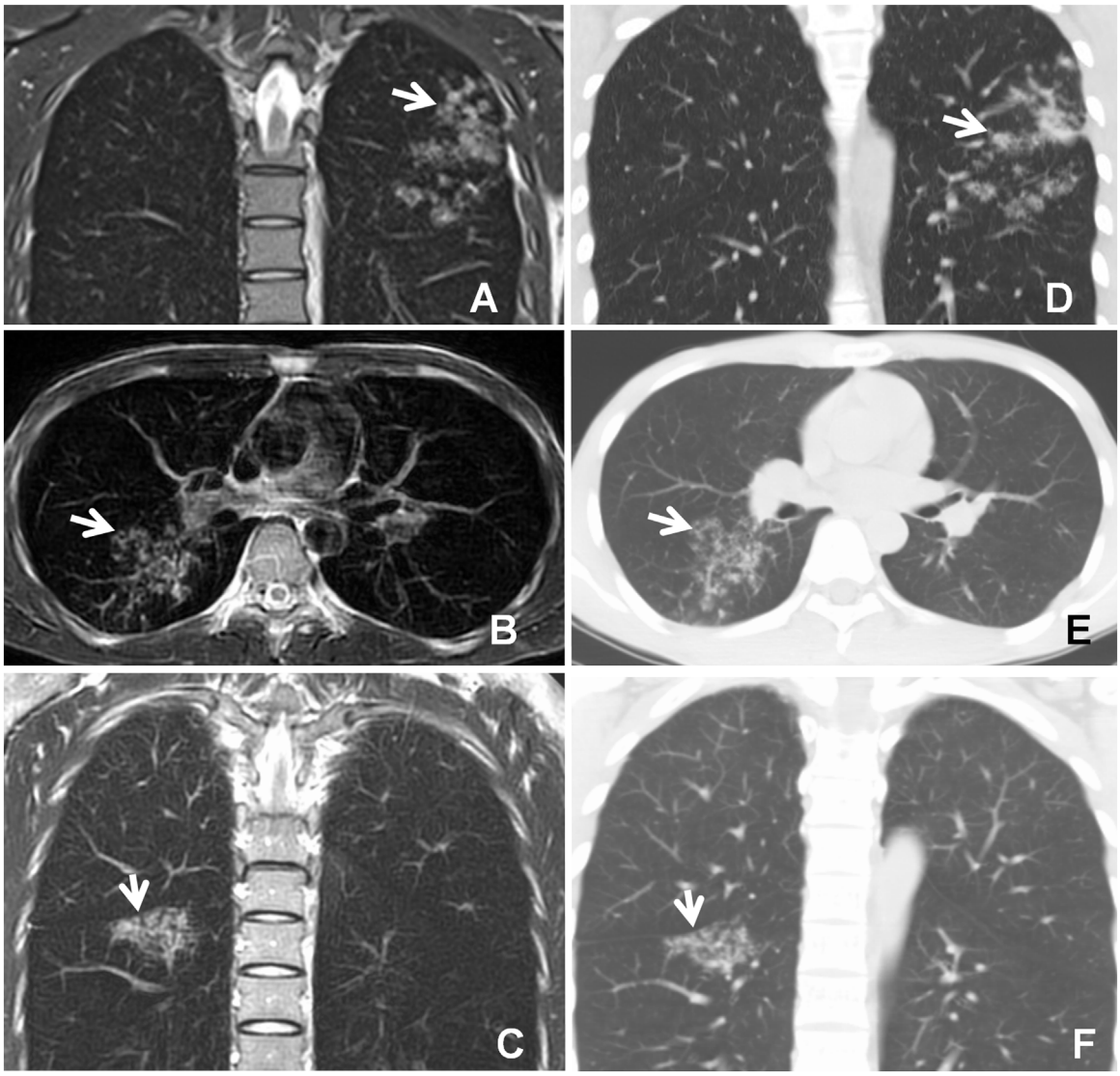

Figure 2. MultiVane improved T2-weighted imaging was able to reveal multiple lesions (arrow), such as centrilobular nodules (A), tree-in-bud sign (B), and multiple centrilobular nodules with interstitial change (C), with image quality comparable to CT images (D, E, and F, respectively). The MRI contrast window was adjusted purposely to that for reading conventional CT images in the evaluation of these lesions.

CT of the same subjects was not able to reveal this caseous necrosis or liquefactive necrosis. The study demonstrated that MRI improved the appearance of cavity or consolidation with a central saturated hypo-signal intensity, peripheral inhomogeneous consolidation, and smooth inner wall without solid mural nodules. These imaging features are consistent with caseous necrosis (Figure 3A). In comparison, CT could only show a homogeneity consolidation in the lung and mediastinal windows (Figure 3B, C). The appearance of central hyper-intensity within inhomogeneous consolidations in T2-weighted imaging with MultiVane (Figure 3D, F) was considered as liquefactive necrosis ($n = 7$), which is different from the appearance of caseosis necrosis. In comparison, liquefactive necrosis lesions were not obvious in CT, which showed only a patchy lesion with soft tissue density (Figure 3E, G). Importantly, detecting caseous necrosis is critical as it indicates active or inactive pulmonary TB in the clinical diagnosis, which is necessary in order to apply the appropriate treatment. In the current study, active ($n = 42$) and inactive ($n = 21$) pulmonary TB cases were identified by both MRI and CT images. Nevertheless, CT is sensitive in detecting small calcified lesions (Figure 3I), which could not be detected by MRI (Figure 3H).

Additionally, MRI provided images that were informative and comparable to CT (Figure 4) for caseous necrosis in a cavity ($n = 11$), as a thin-walled cavity with peripheral consolidation and multiple centrilobular nodules was shown in coronal (Figure 4A) and axial (Figure 4B) sections. These findings are closely related to TB infection.

Moreover, MRI had advantages in the detection of mild pleural thickening or slight hydrothorax compared with CT. In the current study, MRI detected 16 cases with slight pleural effusion or hidden hydrothorax within consolidation versus seven detected by CT ($\kappa = 0.52$). The abnormality presented as a sickle-shaped hyper-intensity along the pleura and adjacent consolidation in MRI (Figure 5A), but with no corresponding pleural abnormality found in CT (Figure 5B).

Detection of nodules and mass by MRI and CT

Based on the cases in the current study, MRI showed excellent agreement with CT in detecting all cases with a mass ($\kappa = 1$) and non-calcified nodules ($\kappa = 0.88–1$), especially for nodule sizes larger than 5 mm, using the number of abnormalities found in CT as

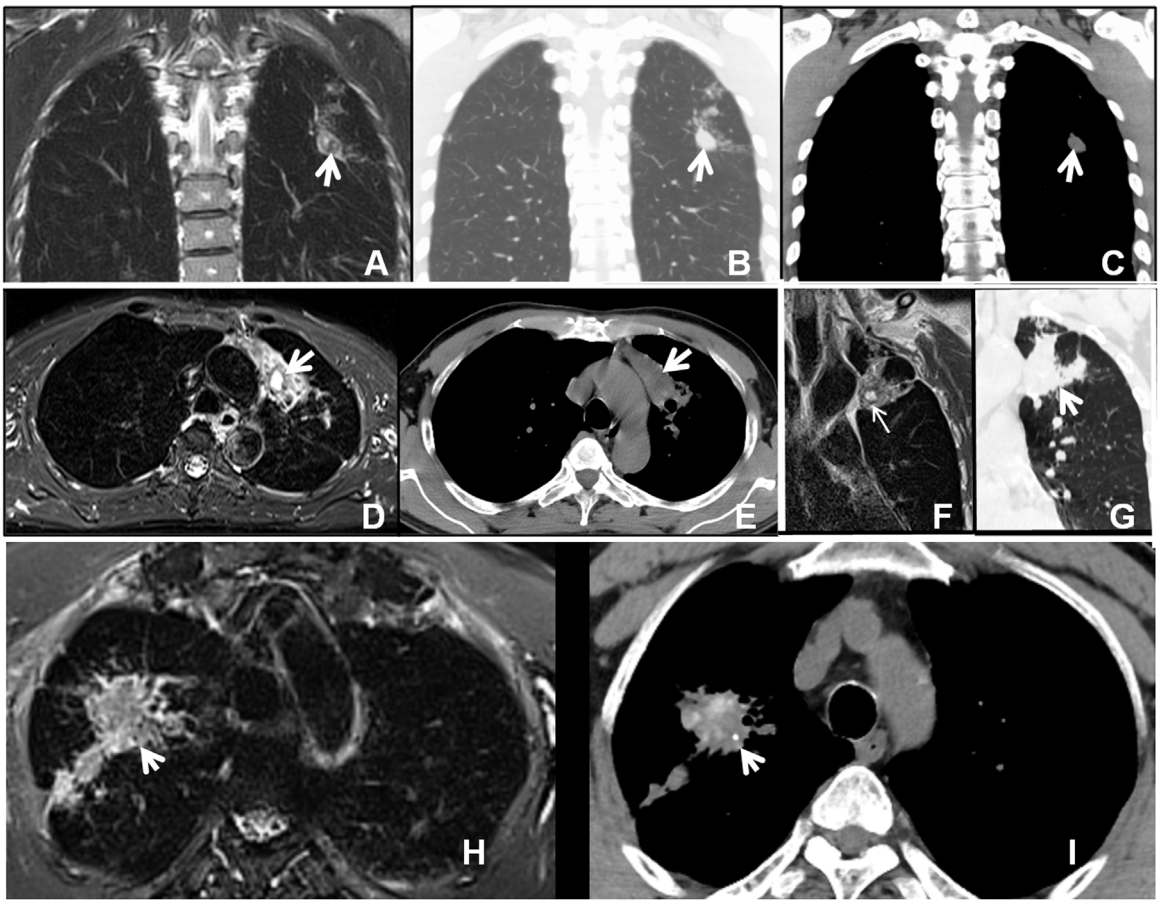

Figure 3. Examples of MRI providing additional imaging features inside consolidation (arrows), such as caseous necrosis(A) and liquefactive necrosis (D and F). These lesions only appeared as a spot or patchy consolidation in the mediastinal window (C and E) and lung window (B and G) in CT images. However, the calcified spots (arrows) within consolidation were found in CT images (I), but not clearly in MRI images (H).

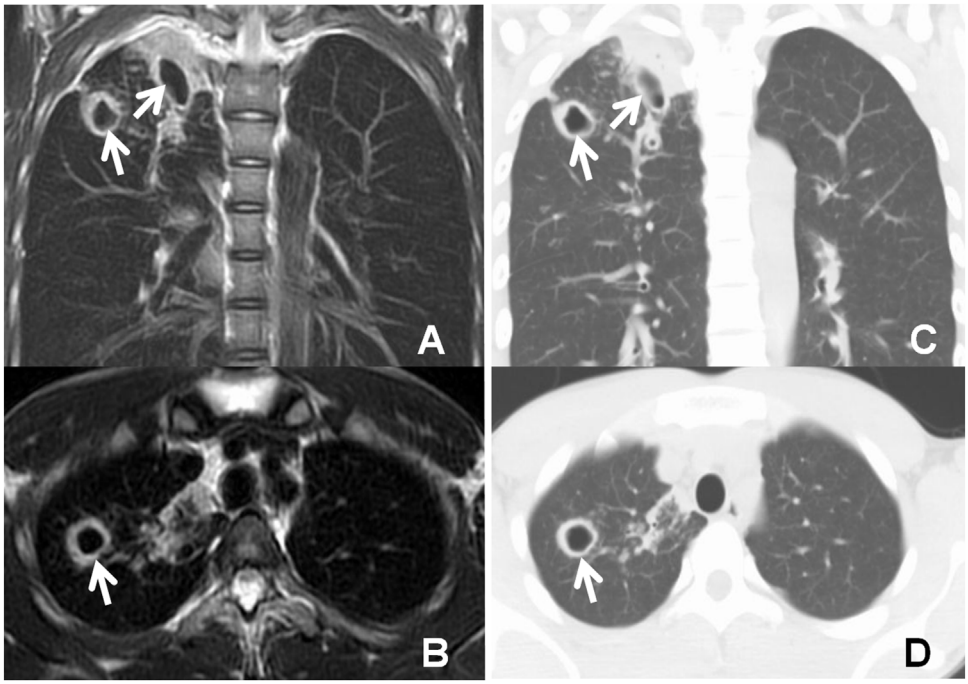

Figure 4. Example of a patient who had two thin-walled cavities (white arrow) with peripheral consolidation and multiple centrilobular nodules in coronal (A) and axial (B) sections. Such MRI findings were comparable to CT (C and D, respectively).

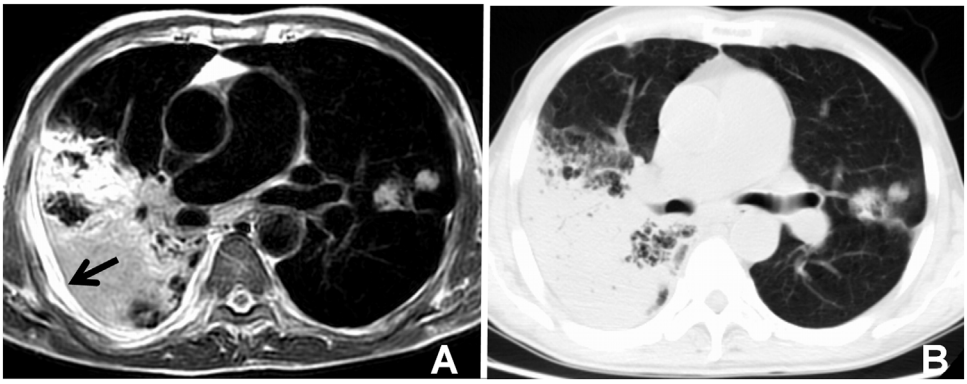

Figure 5. Example of slight pleural effusion. MRI clearly depicted the abnormality as sickle-shaped hyper-intensity along the pleura and adjacent consolidation (black arrow in A), but with no corresponding pleural abnormality in CT (B).

the reference. Unlike CT, calcified nodules had fairly low contrast to the background of lung tissue in T2-weighted MRI (Figure 6). The ability and sensitivity of MRI in detecting nodules or mass increased significantly in proportion to the size for non-calcified nodules ($p = 0.001$), completely calcified nodules ($p = 0.001$; Figure 6A–C), and partially calcified nodules ($p = 0.003$; Figure 6D–F). Details are summarized in Table 4.

Discussion

One of the major challenges of lung imaging by MRI is the inherited motion artifacts caused by respiratory and cardiac motions. Earlier lung MRI studies were typically performed with the standard T2-weighted TSE fat-suppressed imaging sequence, in which a long TR with Cartesian k-space sampling is used. Such a scanning protocol is susceptible to motion artifacts. MultiVane is an advanced motion correction technique with non-Cartesian image sampling and reconstruction using rotating blades in the k-space to detect in-plane motion. It was introduced for use in liver and lung cancer screening to reduce motion-related artifacts, but has seldom been used in pulmonary TB (Kang et al., 2015; Meier-Schroers et al., 2018; Meier-Schroers et al., 2016). In this study, it was found that the advanced MultiVane technique with free breathing could significantly reduce motion artifacts, resulting in improved lung MRI image quality and increased detection of lung lesions, which is consistent with the results of previous reports (Meier-Schroers et al., 2016; Pandit et al., 2011). The optimized lung MRI protocol is not only simplified with a shortened acquisition time, but is also available in many clinical systems (Biederer et al., 2012). The current study demonstrated that T2-weighted imaging with MultiVane implemented can be used to detect MRI signal features of pulmonary TB without breath-holding, which is especially suitable for children, pregnant women, and the elderly.

Lung MRI was comparable to CT in the identification of most signal changes of pulmonary TB, such as consolidation, nodule, cavitation, tree-in-bud sign, interstitial change, ground-glass opacity, and finger-in-glove sign. Attenberger et al. (Attenberger et al., 2014) reported that lung MRI detected 6 false-negative and 11 false-positive lesions with ground-glass opacity. MRI might be false-negative in the detection of ground-glass opacity by depicting such lesions as a nodule, mass, or consolidation, as infectious lesions contain plenty of water. When a lesion contains a minimal amount of water, it could be difficult to identify in the hazy background of the lung due to the relatively low SNR on MRI. On the other hand, respiratory and cardiac artifacts might still also

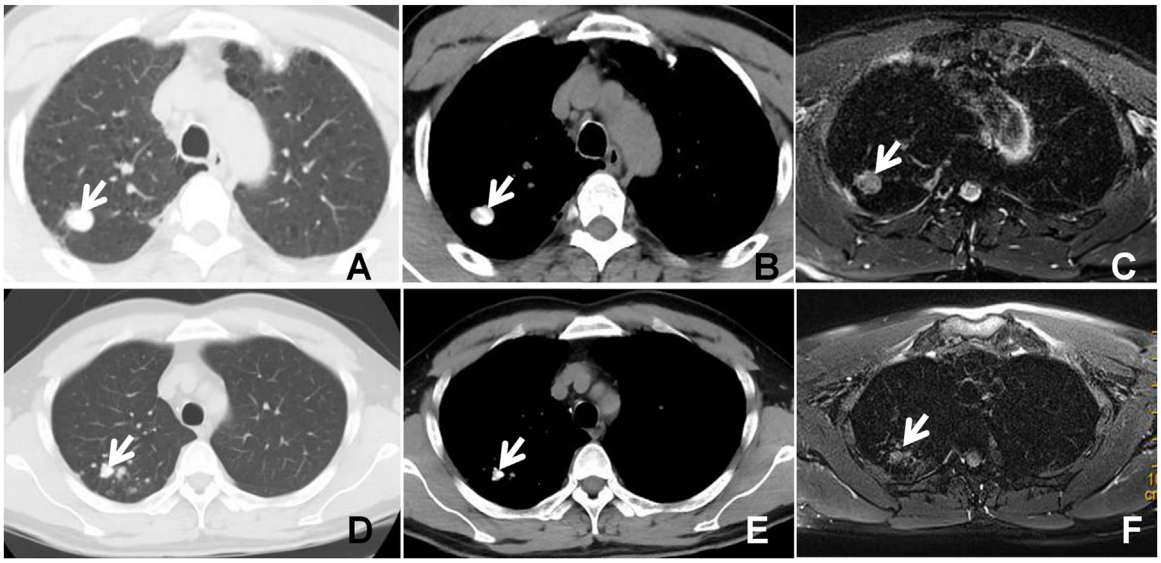

Figure 6. CT images clearly show the completely calcified nodule in the right upper lobe with lung window (A) and mediastinal window (B), which correspond to a slight low signal intensity nodule on T2-weighted TSE images (C). Partially calcified nodules in the upper lobe of the right lung are seen with lung window (D) and mediastinal window (E), which are depicted as relatively hypo-intense nodules with heterogeneity in T2-weighted TSE images (F).

Table 4
Sensitivity of MRI in detecting different types of nodules of different size.

Nodule type	CT[a]	MRI[a]	MRI sensitivity with 95% CI	Chi-square test, *p*-value
Total nodules (Non-calcified nodules)	151	112	74.2% (66.3–80.8%)	
Nodule <5 mm	68	34	50.0% (37.7–62.3%)	0.00*
Nodule 5–10 mm	56	51	91.1% (79.6–96.7%)	
Nodule >10 mm	27	27	100% (84.5–100%)	
Total nodules (Completely calcified nodules)	75	12	16.0% (8.9–26.7%)	
Nodule <5 mm	44	0	0.0% (0.0–10.0%)	0.00*
Nodule 5–10 mm	17	5	29.4% (11.4–56.0%)	
Nodule >10 mm	14	7	50.0% (24.0–76.0%)	
Total nodules (Partially calcified nodules)	49	28	57.1% (42.3–70.9%)	
Nodule <5 mm	22	7	31.8% (14.7–54.9%)	0.02*
Nodule 5–10 mm	14	10	71.4% (42.0–90.4%)	
Nodule >10 mm	15	13	86.7% (58.4–97.7%)	

MRI, magnetic resonance imaging; CT, computed tomography; CI, confidence interval.
[a] CT and MRI numbers indicted separately are the numbers of nodules detected by CT or MRI.

be the cause of a false-positive result. The present study only found one case of false-negative ground-glass opacity and there was no false-positive finding of ground-glass opacity.

Moreover, lung MRI had significant advantages in providing TB-specific information. Caseous necrosis is a form of cell death in which the tissue maintains a cheese-like appearance, and this is encountered in the foci of TB infections. The appearance of a central saturated signal associated with peripheral hyper-intensity may be suggestive of caseous necrosis (De Backer et al., 2007). Liquefactive necrosis is a type of necrosis with transformation of the tissue into a liquid viscous mass and a fluid-filled space (Kumar et al., 2005). MRI is sensitive for the detection of lesions with abundant water, such as related liquefactive necrosis based on the MR signal.

Based on the lesion signal intensity on T2-weighted images, MRI can be used to predict different pathological stages or changes in the pulmonary TB process with (1) slight hyper-intensity possibly reflecting the exudative inflammatory stage; (2) high hyper-intensity inside the lesions indicating liquefactive necrosis; (3) central iso-intensity associated with peripheral hyper-intensity indicating caseous necrosis; (4) relatively hypo-intense areas inside the lesions indicating a relatively cellular fibrotic stage; and (5) hypo-intensity or hypo-intensity inside relative hyper-intensity indicating cure stage with calcification (De Backer et al., 2007; Moon et al., 1996). Some MRI features, such as tree-in-bud and caseous necrosis, may indicate active TB, while fibrotic or calcified lesions with hypo-intensity may suggest inactive pulmonary TB.

With sufficient spatial resolution, MRI can be used to detect a nodule as small as 5 mm (Heye et al., 2012). However, the detection of lesions smaller than 5 mm, especially less than 2–3 mm, is difficult with lung MRI. This is probably because of a susceptibility difference at the interface between the nodule and proton-sparse lung parenchyma. Motion artifacts, a thick slice thickness (5 mm was used in this protocol), or the composition of the nodules themselves, may also contribute to the difficulties in detecting these lesions. Currently, there is a lack of well-established criteria for diagnosing calcification by MRI. Further studies and technical developments are needed to investigate and define the MRI appearance of pulmonary calcification.

In conclusion, this study demonstrated that lung MRI with the MultiVane technique provides motion-reduced high-resolution images of the lung, allowing the characterization of different pulmonary TB lesions without the concerns of radiation exposure associated with CT. Although MRI is less desirable when used to detect small nodules and the nodules with calcification, the MRI protocol and technique applied in this study generally provided acceptable image quality and diagnostic performance for the evaluation of most TB cases, with good agreement with routine clinical CT examinations. Therefore, it offers a promising alternative to the clinical standard CT in the diagnosis and characterization of pulmonary TB.

Acknowledgements

We gratefully acknowledge the China Scholarship Council for the scholarship support to Zhou Liu for his joint PhD dissertation research at Emory University School of Medicine, USA.

Ethical approval

The study was approved by the ethics committee of the People's Hospital of Longhua, Shenzhen, Guangdong, China.

Conflict of interest

Qingping Gu is employed by Philips Medical Systems Greater China. All other authors declare that no competing interests exist.

Author contributions

Liya Wang and Hui Mao: study design and supervision, manuscript integrity and revision; Jianbing Zeng: MRI operation and data collection; Zhou Liu: data analysis and manuscript writing; Zhiqing Wu: lung CT and MRI operation; Guanle Shen: recruited and recommended pulmonary tuberculosis patients; Yuzhong Zhang, Li Li, and Dehong Luo: evaluated and validated lung MRI and CT findings; Qingping Gu: optimized the lung MRI sequence. All authors reviewed this manuscript critically and approved its final submission.

References

Attenberger UI, Morelli JN, Henzler T, Buchheidt D, Fink C, Schoenberg SO, et al. 3 Tesla proton MRI for the diagnosis of pneumonia/lung infiltrates in neutropenic patients with acute myeloid leukemia: initial results in comparison to HRCT. Eur J Radiol 2014;83(1):e61–6.
Biederer J, Beer M, Hirsch W, Wild J, Fabel M, Puderbach M, et al. MRI of the lung (2/3). Why .. when .. how?. Insights Imaging 2012;3(4):355–71.
Chung JH, Huitt G, Yagihashi K, Hobbs SB, Faino AV, Bolster Jr. BD, et al. Proton magnetic resonance imaging for initial assessment of isolated *Mycobacterium avium* complex pneumonia. Ann Am Thorac Soc 2016;13(1):49–57.
Chung JH, Little BP, Forssen AV, Yong J, Nambu A, Kazlouski D, et al. Proton MRI in the evaluation of pulmonary sarcoidosis: comparison to chest CT. Eur J Radiol 2013;82(12):2378–85.

Cutillo AG, Goodrich KC, Ganesan K, Watanabe S, Ailion DC, Morris AH, et al. Alveolar air/tissue interface and nuclear magnetic resonance behavior of normal and edematous lungs. Am J Respir Crit Care Med 1995;151(4):1018–26.
De Backer AI, Mortele KJ, Van Den Heuvel E, Vanschoubroeck IJ, Kockx MM, Van de Vyvere M. Tuberculous adenitis: comparison of CT and MRI findings with histopathological features. Eur Radiol 2007;17(4):1111–7.
Dewes P, Frellesen C, Al-Butmeh F, Albrecht MH, Scholtz JE, Metzger SC, et al. Comparative evaluation of non-contrast CAIPIRINHA-VIBE 3T-MRI and multi-detector CT for detection of pulmonary nodules: In vivo evaluation of diagnostic accuracy and image quality. Eur J Radiol 2016;85(1):193–8.
Eibel R, Herzog P, Dietrich O, Rieger CT, Ostermann H, Reiser MF, et al. Pulmonary abnormalities in immunocompromised patients: comparative detection with parallel acquisition MR imaging and thin-section helical CT. Radiology 2006;241(3):880–91.
Ekinci A, Yucel Ucarkus T, Okur A, Ozturk M, Dogan S. MRI of pneumonia in immunocompromised patients: comparison with CT. Diagn Interv Radiol 2017;23(1):22–8.
Heye T, Ley S, Heussel CP, Dienemann H, Kauczor HU, Hosch W, et al. Detection and size of pulmonary lesions: how accurate is MRI? A prospective comparison of CT and MRI. Acta Radiol 2012;53(2):153–60.
Iwasawa T, Takahashi H, Ogura T, Asakura A, Gotoh T, Kagei S, et al. Correlation of lung parenchymal MR signal intensity with pulmonary function tests and quantitative computed tomography (CT) evaluation: a pilot study. J Magn Reson Imaging 2007;26(6):1530–6.
Kang KA, Kim YK, Kim E, Jeong WK, Choi D, Lee WJ, et al. T2-weighted liver MRI using the multivane technique at 3T: comparison with conventional T2-weighted MRI. Korean J Radiol 2015;16(5):1038–46.
Kumar V, Abbas AK, Fausto N, Aster JC. Robbins and Cotran pathologic basis of disease. Philadelphia: Elsevier Saunders; 2005.
Landis JR, Koch GG. The measurement of observer agreement for categorical data. Biometrics 1977;33(1):159–74.
Leutner CC, Gieseke J, Lutterbey G, Kuhl CK, Glasmacher A, Wardelmann E, et al. MR imaging of pneumonia in immunocompromised patients: comparison with helical CT. Am J Roentgenol 2000;175(2):391–7.
Liszewski MC, Gorkem S, Sodhi KS, Lee EY. Lung magnetic resonance imaging for pneumonia in children. Pediatr Radiol 2017;47(11):1420–30.
Meier-Schroers M, Homsi R, Skowasch D, Buermann J, Zipfel M, Schild HH, et al. Lung cancer screening with MRI: results of the first screening round. J Cancer Res Clin Oncol 2018;144(1):117–25.
Meier-Schroers M, Kukuk G, Homsi R, Skowasch D, Schild HH, Thomas D. MRI of the lung using the PROPELLER technique: artifact reduction, better image quality and improved nodule detection. Eur J Radiol 2016;85(4):707–13.
Moon WK, Im JG, Yu IK, Lee SK, Yeon KM, Han MC. Mediastinal tuberculous lymphadenitis: MR imaging appearance with clinicopathologic correlation. Am J Roentgenol 1996;166(1):21–5.
Muller NL. Computed tomography and magnetic resonance imaging: past, present and future. Eur Respir J Suppl 2002;35:3s–12s.
Nagel SN, Wyschkon S, Schwartz S, Hamm B, Elgeti T. Can magnetic resonance imaging be an alternative to computed tomography in immunocompromised patients with suspected fungal infections? Feasibility of a speed optimized examination protocol at 3 Tesla. Eur J Radiol 2016;85(4):857–63.
World Health Organization. Global tuberculosis report 2016. 2016.
Ozcan HN, Gormez A, Ozsurekci Y, Karakaya J, Oguz B, Unal S, et al. Magnetic resonance imaging of pulmonary infection in immunocompromised children: comparison with multidetector computed tomography. Pediatr Radiol 2017;47(2):146–53.
Pandit P, Qi Y, King KF, Johnson GA. Reduction of artifacts in T2 -weighted PROPELLER in high-field preclinical imaging. Magn Reson Med 2011;65(2):538–43.
Puderbach M, Eichinger M, Haeselbarth J, Ley S, Kopp-Schneider A, Tuengerthal S, et al. Assessment of morphological MRI for pulmonary changes in cystic fibrosis (CF) patients: comparison to thin-section CT and chest x-ray. Invest Radiol 2007;42(10):715–25.
Rizzi EB, Schinina V, Cristofaro M, Goletti D, Palmieri F, Bevilacqua N, et al. Detection of Pulmonary tuberculosis: comparing MR imaging with HRCT. BMC Infect Dis 2011;11:243.
Wielputz M, Kauczor HU. MRI of the lung: state of the art. Diagn Interv Radiol 2012;18(4):344–53.
Wild JM, Marshall H, Bock M, Schad LR, Jakob PM, Puderbach M, et al. MRI of the lung (1/3): methods. Insights Imaging 2012;3(4):345–53.